Iron Heterogeneity in Early Active Multiple Sclerosis Lesions

Mylyne Tham, MSc,[1] Josa M. Frischer, MD, PhD,[2] Stephen D. Weigand, MSc,[3] Patrick D. Fitz-Gibbon, MSc,[3] Samuel M. Webb, PhD,[4] Yong Guo, MD, PhD,[5] Reginald C. Adiele, PhD,[1] Christopher A. Robinson, MD,[6] Wolfgang Brück, MD,[7] Hans Lassmann, PhD,[8] Kendra L. Furber, PhD,[1] M. Jake Pushie, PhD,[9] Joseph E. Parisi, MD,[10] Claudia F. Lucchinetti, MD,[5] and Bogdan F. Popescu, MD, PhD [1]

Objective: Multiple sclerosis (MS) is a heterogeneous inflammatory demyelinating disease. Iron distribution is altered in MS patients' brains, suggesting iron liberation within active lesions amplifies demyelination and neurodegeneration. Whether the amount and distribution of iron are similar or different among different MS immunopatterns is currently unknown.

Methods: We used synchrotron X-ray fluorescence imaging, histology, and immunohistochemistry to compare the iron quantity and distribution between immunopattern II and III early active MS lesions. We analyzed archival autopsy and biopsy tissue from 21 MS patients.

Results: Immunopattern II early active lesions contain 64% more iron (95% confidence interval [CI] = 17–127%, $p = 0.004$) than immunopattern III lesions, and 30% more iron than the surrounding periplaque white matter (95% CI = 3–64%, $p = 0.03$). Iron in immunopattern III lesions is 28% lower than in the periplaque white matter (95% CI = −40 to −14%, $p < 0.001$). When normalizing the iron content of early active lesions to that of surrounding periplaque white matter, the ratio is significantly higher in immunopattern II ($p < 0.001$). Microfocused X-ray fluorescence imaging shows that iron in immunopattern II lesions localizes to macrophages, whereas macrophages in immunopattern III lesions contain little iron.

Interpretation: Iron distribution and content are heterogeneous in early active MS lesions. Iron accumulates in macrophages in immunopattern II, but not immunopattern III lesions. This heterogeneity in the two most common MS immunopatterns may be explained by different macrophage polarization, origin, or different demyelination mechanisms, and paves the way for developing new or using existing iron-sensitive magnetic resonance imaging techniques to differentiate among immunopatterns in the general nonbiopsied MS patient population.

ANN NEUROL 2021;89:498–510

Significant advancements in understanding the pathogenesis and evolution of multiple sclerosis (MS), and its clinical, pathological, and radiological features, have further refined the definition of MS. Poser et al postulated in 1982 that MS may not be a single disease.[1] In support of this hypothesis, pathology has shown that the

View this article online at wileyonlinelibrary.com. DOI: 10.1002/ana.25974

Received Jun 4, 2020, and in revised form Nov 23, 2020. Accepted for publication Nov 23, 2020.

Address correspondence to Dr Lucchinetti, Department of Neurology, Mayo Clinic, 200 First St SW, Rochester, MN 55905, E-mail: clucchinetti@mayo.edu; or Dr Popescu, Cameco MS Neuroscience Research Centre, University of Saskatchewan, Saskaton City Hospital, 701 Queen St, Saskatoon, Saskatchewan S7K 0M7, Canada, E-mail: bogdan.popescu@usask.ca

From the [1]Department of Anatomy, Physiology, and Pharmacology/Cameco MS Neuroscience Research Centre, College of Medicine, University of Saskatchewan, Saskatoon, Saskatchewan, Canada; [2]Department of Neurosurgery, Medical University Vienna, Vienna, Austria; [3]Department of Health Sciences Research, College of Medicine, Mayo Clinic, Rochester, MN, USA; [4]Stanford Synchrotron Radiation Lightsource, SLAC National Accelerator Laboratory, Menlo Park, CA, USA; [5]Department of Neurology, College of Medicine, Mayo Clinic, Rochester, MN, USA; [6]Department of Pathology and Laboratory Medicine, Saskatoon Health Region/College of Medicine, University of Saskatchewan, Saskatoon, Saskatchewan, Canada; [7]Department of Neuropathology, University of Göttingen, Göttingen, Germany; [8]Department of Neuroimmunology, Center for Brain Research, Medical University of Vienna, Vienna, Austria; [9]Department of Surgery, Division of Neurosurgery, College of Medicine, University of Saskatchewan, Saskatoon, Saskatchewan, Canada; and [10]Department of Laboratory Medicine and Pathology, Mayo Clinic, Rochester, MN, USA

immunopathology of early active MS lesions is heterogeneous.[2] This pathological heterogeneity suggests that the targets of injury and mechanisms of demyelination may be different in disease subgroups and has resulted in recognition of 4 distinct immunopatterns (IPs). Although pathologic heterogeneity is observed among MS patients, IPs in multiple active lesions from a single patient are identical.[2] Furthermore, immunopathological patterns persist in active lesions sampled at different time points from the same MS patient, reinforcing the concept of patient-dependent immunopathological heterogeneity in early MS.[3]

Data from several laboratories support the pathogenic heterogeneity concept in early MS. Distinct cellular expression patterns of the chemokine receptors CCR1 and CCR5 thought to reflect the differential activation of mononuclear phagocytes have been observed in lesions from patients with IP II and IP III MS.[4] Defects of mitochondrial respiratory chain complex IV in oligodendrocytes, reactive astrocytes and axons,[5] severe oxidative damage,[6] and myeloperoxidase and inducible nitric oxide synthase expressing microglia associated with upregulation of proteins involved in tissue preconditioning[7] are characteristic for IP III but not IP II MS active lesions. Tissue response to therapeutic plasma exchange also appears to be different, with plasma exchange benefiting some patients with IP II, but not with IP III.[8,9] Although the efficacy of various therapies currently available for MS has not been studied by taking into consideration the pathological IPs of MS patients, it is possible that the presence of different immunopathological patterns may be at least partially responsible for the variation in response, not only to B-cell–depleting therapy, but also to various alternative approaches that are used, apart from plasma exchange, to treat aggressive MS.[10,11]

The concept of pathologic heterogeneity has been challenged.[12–14] Some studies suggest that the earliest pathologic changes are the prephagocytic lesions, pattern III-like lesions with widespread oligodendrocyte apoptosis on a background of microglial activation and myelin preservation, followed by superimposed pattern II-like demyelination and complement activation.[12] We have recently reported that a subset of active demyelinating neuromyelitis optica supraspinal lesions simultaneously show overlapping pathological features of pattern II (antibody deposition and complement activation) and pattern III (oligodendrocyte apoptosis with preferential loss of myelin-associated glycoprotein) MS.[15] These findings, coupled with the aggressive clinical course in the index pediatric patient case illustrated in the study with an episode of myelitis, severe brain stem dysfunction, relapse-related disability and rapid death, raise the possibility that the index case described by Barnett and Prineas is neuromyelitis optica rather than MS.[12,15] Others suggest that the dominant mechanism of demyelination in all lesions is antibody- and complement-mediated myelin phagocytosis.[13,14] However, these studies analyze lesions from MS patients with longstanding disease (median disease duration > 22 and 26 years, respectively) and use different classifications of lesion activity.[13,14] Early active lesions are the prerequisite for IP classification, and they rarely occur in chronic MS.[2,16] Therefore, it is unlikely that early active lesions were available for analysis in these studies.

Recent neuropathological data have reported altered distribution of iron in the brains of MS patients[17–20] and suggest that the liberation of iron within active lesions may accentuate demyelination and neurodegeneration.[18] However, the precise role of metals and metalloproteins in acute MS remains controversial. This is the first systematic report to study the iron heterogeneity in MS by IP. We use X-ray fluorescence imaging (XFI) to compare the distribution and quantification of iron in early active lesions and periplaque white matter (PPWM) between the 2 most common MS IPs (IP II and IP III), which together comprise 80% of all MS patients.

Patients and Methods

Sample Characterization

Study approval was granted by the University of Saskatchewan Biomedical Research Ethics Board (Bio# 11–217, Bio# 11–104), Mayo Clinic Institutional Review Board (IRB-2067-99), and Center of Brain Research, Medical University of Vienna, Austria (EK Nr. 535/2004/2019). We analyzed formalin-fixed paraffin-embedded archival autopsy and biopsy tissue from 21 MS patients (Table 1). Tissue was embedded in paraffin under routine neuropathology processing, therefore limiting variability between cases with respect to fixation duration. A certified neurologist determined the clinical diagnosis according to McDonald or Poser criteria.[21,22] Clinical course was defined as clinically isolated syndrome, acute monophasic MS with death within 1 year, relapsing–remitting MS, secondary progressive MS, or uncertain clinical course, when insufficient clinical data rendered subclassification impossible.

Neuropathology and Immunohistochemistry

A certified neuropathologist confirmed the pathological diagnosis of inflammatory demyelination consistent with MS. Five-micrometer-thick microscopic sections were stained with hematoxylin and eosin for morphological evaluation, Luxol fast blue/periodic acid–Schiff or Luxol fast blue/hematoxylin and eosin for myelin, and silver impregnation for axons. Immunohistochemistry was performed

TABLE 1. Acute Case Reference Table

Case #	IP Class	Autopsy or Biopsy	Gender	Age, yr	Disease Duration, mo	ROIs, n
1	2	B	F	9	NA	2
2	2	B	F	37	156	3
3	2	A	M	46	9	2
4	2	A	F	50	96	4
5	2	B	F	68	1	2
6	2	B	M	69	1.8	1
7	2	A	M	71	144	5
8	2	B	M	72	0.1	6
9	3	A	F	17	0.5	4
10	3	A	M	28	0.8	4
11	3	A	F	28	2	5
12	3	B	M	33	NA	2
13	3	A	F	34	13	4
14	3	A	M	35	1.5	4
15	3	B	M	37	1.8	1
16	3	B	M	38	0.3	1
17	3	A	F	40	120	5
18	3	A	F	45	0.2	3
19	3	A	M	45	0.6	5
20	3	A	M	58	3	1
21	3	A	M	78	2	4

A = autopsy; B = biopsy; F = female; IP = immunopattern; M = male; NA = not available; ROI = region of interest.

using an avidin–biotin technique and primary antibodies against myelin proteolipid protein (PLP; rabbit polyclonal; 1:500; Serotec, Oxford, UK), myelin oligodendrocyte glycoprotein (rabbit monoclonal; 1:1,000; Abcam, Cambridge, MA), myelin-associated glycoprotein (rabbit monoclonal; 1:500; Sigma, St Louis, MO), macrophages/microglia (CD68; mouse monoclonal; 1:1,000; Dako, Glostrup, Denmark), all T lymphocytes (CD3; rat monoclonal; 1:400; Serotec), cytotoxic T lymphocytes (CD8; mouse monoclonal; 1:50; Dako), phosphorylated neurofilament (rabbit polyclonal; 1:2,000; Chemicon International, Temecula, CA), ferritin heavy chain (rabbit polyclonal; 1:1,000; Abcam), complement C9neo antigen (mouse monoclonal; 1:200; Prof Morgan, Cardiff, UK), terminal complement complex (TCC) and C9 (rabbit polyclonal antihuman; 1:200; Prof Morgan), and TCC and C9 (rabbit polyclonal antirat; 1:200; Prof Morgan).

Active white matter lesions were classified as described previously.[23] Macrophages (see Fig 1E, K) in early active white matter lesions contained myelin debris immunoreactive for minor and major myelin proteins (see insets in Fig 1B, H). Macrophages in late active lesions contained myelin degradation products immunoreactive for only major myelin protein. PPWM referred to the white matter immediately surrounding the demyelinated lesion (<2mm away from the lesion edge).[16] Normal-appearing white matter, located at least 2mm away from the lesion,[16] was only present in one block (see Fig 1B) and therefore not analyzed.

Early active lesions were next classified into IP II and IP III according to published criteria.[2] IP II lesions were characterized by active demyelination with equal losses of all myelin proteins (see Figs 1B-D and 2B, C), associated with immunoglobulin and complement deposition (see Figs 1F and 2D) on myelin (see lower left inset

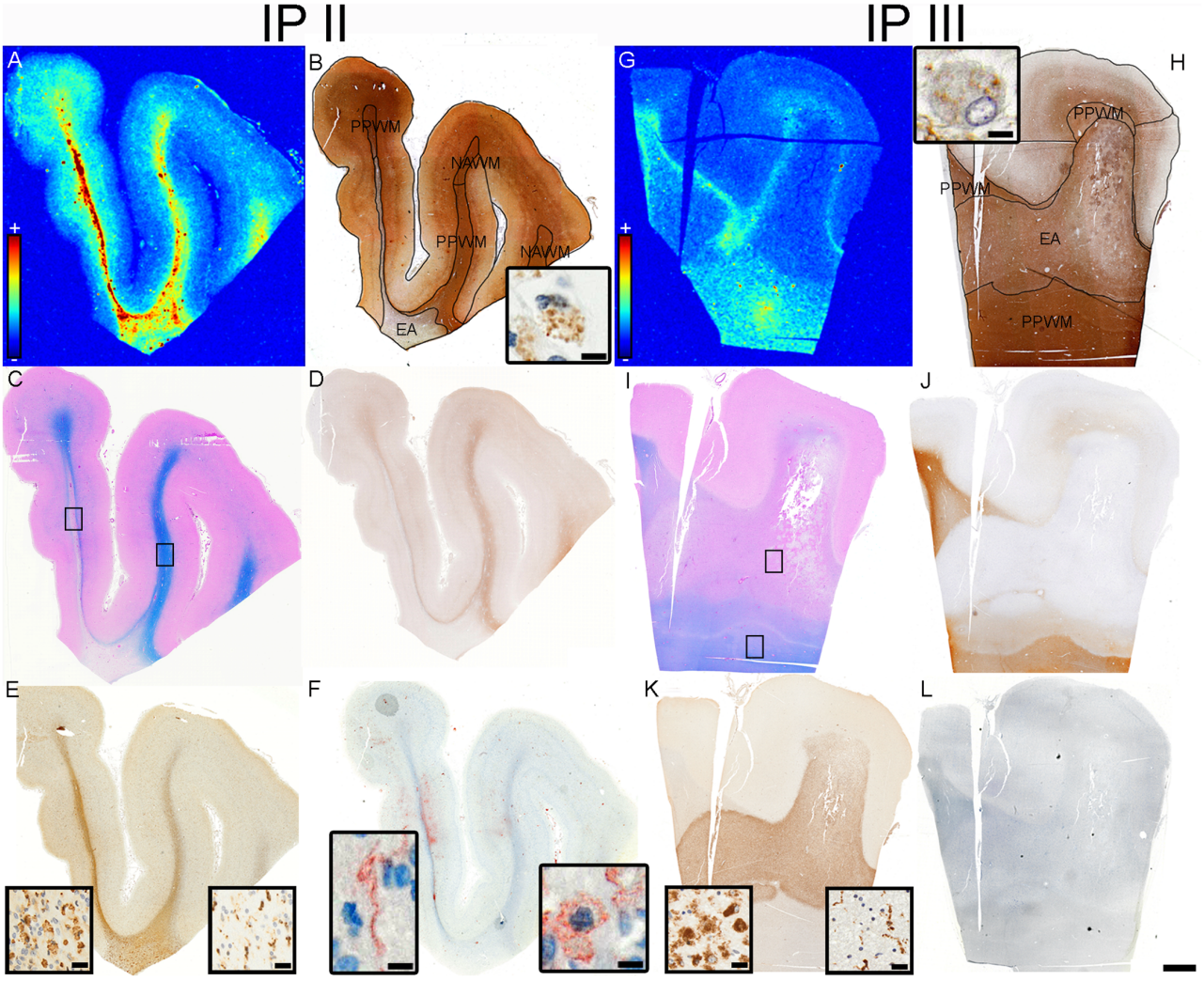

FIGURE 1: Iron in early active (EA) multiple sclerosis (MS) lesions: (A–F) Immunopattern (IP) II MS (Case 7 in Table 1 and Fig 3A; first block). (G–L) IP III MS (Case 9 in Table 1 and Fig 3A). (A) Iron is increased in IP II EA lesions (X-ray fluorescence imaging [XFI]). (B) The circumscribed loss of proteolipid protein (PLP) immunoreactivity highlights demyelination; the various regions of interest are outlined and named (EA = early active lesion; LA = late active lesion; NAWM = normal-appearing white matter; PPWM = periplaque white matter) on this map (PLP); inset shows the presence of myelin oligodendrocyte glycoprotein (MOG) immunoreactive myelin debris within macrophages (MOG). (C) The lack of Luxol fast blue (Lfb) staining indicates demyelination; the areas imaged with microfocused XFI (see Fig 4A, B, E, F) are indicated (*rectangles*) on this map (Lfb/hematoxylin and eosin [HE]). (D) Loss of myelin-associated glycoprotein (MAG) is equal to loss of PLP (compare with B; MAG). (E) The lesion is infiltrated by activated macrophages (higher magnification shown in lower left panel); activated microglia are present in the PPWM (higher magnification shown in lower right panel; KiM1P). (F) Complement deposition is present within the lesion, on myelin (lower left panel) and within macrophages (lower right panel; C9neo). (G) Iron is decreased in IP III EA lesions (XFI). (H) PLP immunoreactivity is still present in the EA lesion; the various regions of interest are outlined and named on this map (PLP); inset shows the presence of MOG immunoreactive myelin debris within macrophages (MOG). (I) Lfb staining is lost in the EA lesion; the areas imaged with microfocused XFI (see Fig 4C, D, G, H) are indicated (*rectangles*) on this map (Lfb/HE). (J) There is preferential loss of myelin-associated glycoprotein (MAG; compare with H; MAG). (K) The lesion is infiltrated by activated macrophages (higher magnification shown in lower left panel); activated microglia are present in the PPWM (higher magnification shown in lower right panel; KiM1P). (L) Complement deposition is not present in lesion (C9neo). Color scales (A, G) represent the normalized total Kα fluorescence counts, proportional to total metal present, from blue (lowest) to red (highest). Scale bars = 3mm. Inset scale bars = 25μm (B, H, F), 75μm (E, K).

in Fig 1F), and macrophage phagocytosis of complement-opsonized myelin debris (see lower right inset in Fig 1F). IP III lesions showed active demyelination with oligodendrocyte apoptosis and preferential loss of myelin-associated glycoprotein (see Figs 1H–J and 2F–H), and no immunoreactivity for complement (see Fig 1L).

Macrophage Counting in Early Active Lesions

We photographed 10 random ×40 fields on slides immunostained for macrophages. Macrophages in each image were counted using the ImageJ cell counter plugin. The area and cellular density were subsequently calculated and used for statistical analysis.

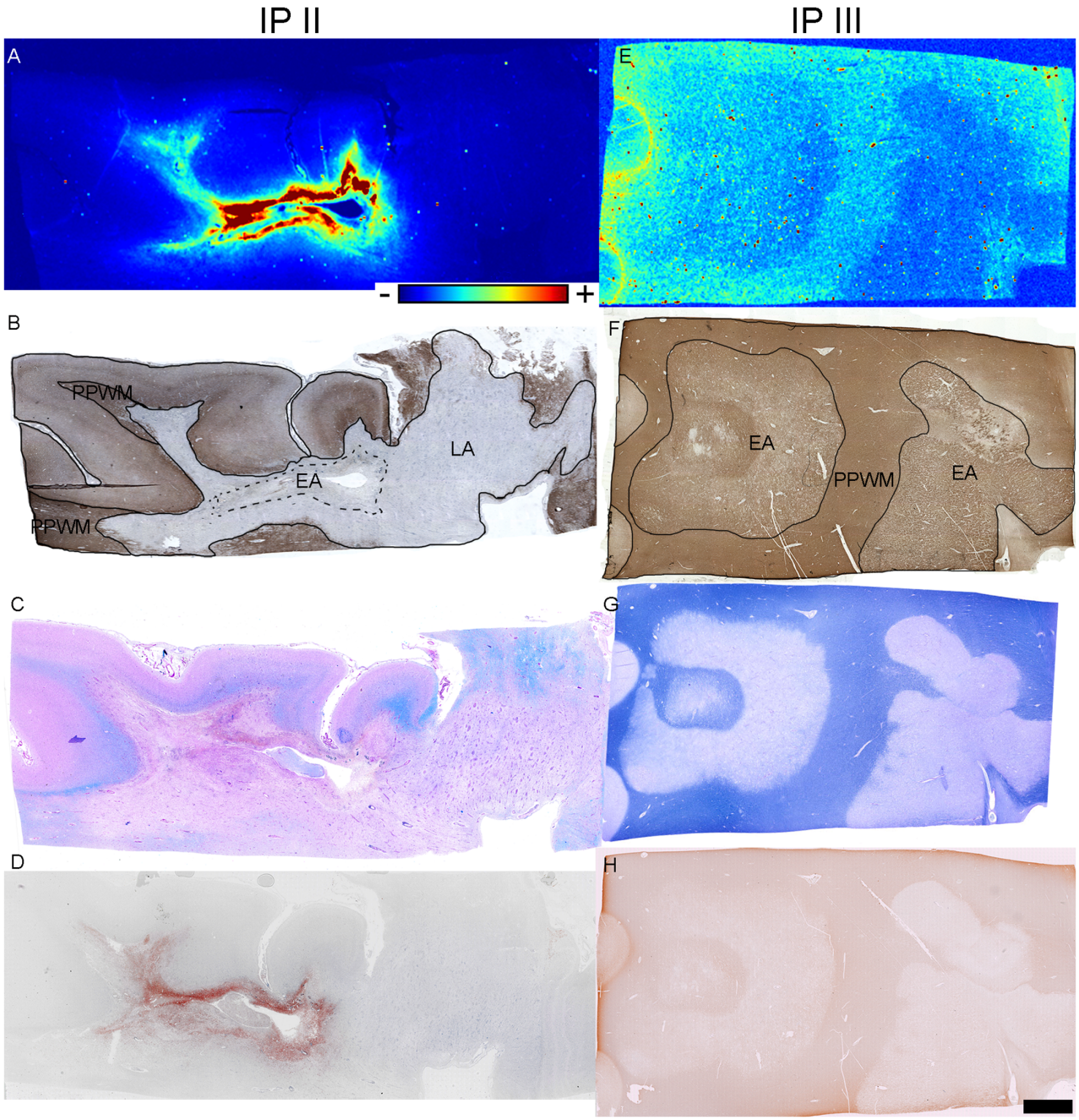

FIGURE 2: Iron in early active (EA) multiple sclerosis (MS) lesions. (A–C) Immunopattern (IP) II MS (Case 4 in Table 1 and Fig 3A); (D–F) IP III MS (Case 11 in Table 1 and Fig 3A; second block). (A) Iron is increased in IP II EA lesions (X-ray fluorescence imaging [XFI]). (B) The lack of proteolipid protein (PLP) immunoreactivity indicates demyelination; the various regions of interest are outlined and named (EA = early active lesion; LA = late active lesion; PPWM = periplaque white matter) on this map (PLP). (C) The lack of Luxol fast blue (Lfb) staining indicates demyelination (Lfb/hematoxylin and eosin [HE]). (D) Complement deposition is present in the EA lesion (C9neo). (E) Iron is decreased in IP III EA lesions (XFI). (F) PLP immunoreactivity is still present in the EA lesions; the various regions of interest are outlined and named on this map (PLP). (G) The lack of Lfb staining indicates demyelination (Lfb/HE). (H) There is preferential loss of myelin-associated glycoprotein (MAG; compare with F; MAG). Color scales (A, E) represent the normalized total Kα fluorescence counts, proportional to total metal present, from blue (lowest) to red (highest). Scale bar = 3mm.

Synchrotron XFI and Chemically Specific XFI

Synchrotron XFI was performed at the Stanford Synchrotron Radiation Lightsource, Stanford University, Menlo Park, California on 15μm-thick sections collected on metal-free plastic coverslips as described previously.[20] Whole sections were imaged on beamline 10–2, mounted at 45° to the 12.5keV incident beam that produced a 50μm × 50μm beamspot on the sample after passing through a glass polycapillary. The beam exposure time was 40ms/pixel. Fluorescent energy windows were centered for iron (6.21–6.70keV).

Regions of interest (ROIs) were imaged at higher resolution using the microfocused XFI beamline 2–3. The incident X-ray beam (7.15keV) was focused with Kirkpatrick–Baez mirrors to produce a 3μm × 3μm spot on the sample. The exposure time was 120ms/pixel dwell time. Fluorescence was normalized against the incident X-ray beam to take into account intensity fluctuations. A silicon drift detector (Hitachi, Tokyo, Japan) mounted at 90° to the incident beam and utilizing the Xpress3 signal processing system (Quantum Detectors, Oxford, UK) detected the X-ray fluorescence. Chemically specific XFI of iron was performed on 4 IP II and 3 IP III cases using incident energies of 7,132.0eV (ferric iron; Fe^{3+}) and 7,126.5eV (ferrous iron; Fe^{2+}).[24]

Histology: XFI Correlation and XFI Data Analysis

Sections stained for myelin were scanned at ×40 magnification using an Olympus (Tokyo, Japan) VS110 slide scanner. Lesion and PPWM ROIs were outlined on whole maps saved as JPEG files (see Figs 1B, H and 2B, F). XFI images were generated using Microprobe Analysis Kit software.[25] Histology and XFI maps were displayed side by side, and XFI ROIs were outlined using histology maps as guides (see Figs 1A, B, G, H and 2A, B, E, F).[20] We converted fluorescence intensities to areal concentrations ($\mu g/cm^2$) using an iron reference standard (Fe, 56.0$\mu g/cm^2$) deposited on a 6.3μm-thick mylar film (Micromatter, Vancouver, BC, Canada).[26] Data were then imported into R for statistical analysis (R Foundation for Statistical Computing, Vienna, Austria, http://R-project.org). The impact of blood iron from large vessels was accounted for by excluding them from the ROI.[20]

Statistical Analysis

We used a very similar 2-stage data analysis approach to that previously reported.[20] The first stage involved calculating iron densities, expressed as $\mu g/cm^2$, across all pixels in a given ROI and calculating the median value across all pixels. The median was preferred to the mean because it is robust to possible outliers. The second stage involved analyzing ROI-level metal densities using standard statistical methods, taking into account the repeated measures across subjects. Our primary analysis used linear mixed effects regression models fitted with the lme4 package in R. The models included subject-specific intercepts, a main effect for age, and an interaction between tissue type (early active, late active, periplaque white matter) and IP. This allowed us to control for age and estimate the difference between IP II and IP III subjects separately for early active, late active, and PPWM tissue. Quantile-based confidence intervals (CIs) for these estimates were obtained from parametric bootstrap sampling using the arm package in R.[27] To report p values from the simulations, we "inverted" quantile-based 95% CIs, a technique justified by the relationship between CIs and p values and because a 95% CI that does not include zero is equivalent to $p < 0.05$. A secondary analysis was limited to subjects with an early active or a late active ROI and an accompanying PPWM ROI to serve as an internal normalizing reference. Separately for early active and late active regions, we calculated the ratio of the iron density in the active regions versus that in the PPWM. For subjects with multiple ROIs, we calculated the mean across their active ROIs and divided it by the mean across their PPWM ROIs. We compared ratios for IP II versus IP III patients using a nonparametric Wilcoxon rank sum/Mann–Whitney U test.

Results

Cohort Characterization

We studied tissues from 21 patients (8 IP II [38%] and 13 IP III [62%] patients; 9 female [43%] and 12 male patients [57%]; see Tables 1 and 2). The median disease duration was 2 months (range = 0–156). The median age at biopsy or death was 40 years (range = 9–78). Four patients (19%) had relapsing–remitting MS, 3 (14%) secondary progressive MS, 8 (38%) acute monophasic MS, and 1 (5%) clinical isolated syndrome. The clinical course was unavailable in 5 cases (24%).

Twenty-six blocks (11 IP II and 15 IP III; 10 biopsies and 16 autopsies) containing 69 ROIs were analyzed: 34 early active white matter lesions (49%), 5 late active white matter lesions (7%), and 30 PPWM (43%; see Tables 1 and 2).

IP II patients tended to be older than IP III patients (median = 59 vs 37 years, $p = 0.08$). Median disease duration was 9 months in IP II patients versus 2 months in IP III patients ($p = 0.24$). Half of IP II patients were women versus 38% of IP III patients ($p = 0.95$). Although not statistically significant ($p = 0.18$), tissue from IP II cases was predominantly from biopsies (62%), whereas tissue from IP III cases was predominantly from autopsies (77%). The median number of analyzed ROIs per case was 2 for IP II patients and 4 for IP III patients ($p = 0.77$; see Table 2).

Iron Content of MS Lesions and PPWM by IP

Early active IP II lesions contained an estimated 64% more iron (95% CI = 17–127%, $p = 0.004$) than early active IP III lesions (see Figs 1A, G, 2A, E, and 3A, B and Table 3) after adjusting for age. Differences in iron content were not statistically significant between IP II and IP III among late active lesions ($p = 0.40$; note the small number of late active lesions), or between IP II and IP III PPWM ($p = 0.54$; see Table 3). These results were adjusted for patient age, because this was found to be an

TABLE 2. Summary of Patient Clinical Characteristics

Characteristic	IP II	IP III	All Cases
Subjects, n	8	13	21
Gender, n (%)			
F	4 (50%)	5 (38%)	9 (43%)
M	4 (50%)	8 (62%)	12 (57%)
Age, yr			
Median	59	37	40
Q1, Q3	44, 70	33, 45	34, 58
Range	9–72	17–78	9–78
Disease duration, mo			
Median	9	2	2
Q1, Q3	1, 120	1, 2	1, 11
Range	0–156	0–120	0–156
Missing	1	1	2
Clinical course, n (%)			
Uncertain/unavailable	2 (25%)	3 (23%)	5 (24%)
RRMS	2 (25%)	2 (15%)	4 (19%)
SPMS with attacks	3 (38%)	0 (0%)	3 (14%)
Monophasic to death within 1 year	0 (0%)	8 (62%)	8 (38%)
Isolated demyelinating syndrome	1 (12%)	0 (0%)	1 (5%)
Regions of interest per patient			
Median	2	4	4
Q1, Q3	2, 4	2, 5	2, 5
Range	1–6	1–5	1–6

F = female; IP = immunopattern; M = male; MS = multiple sclerosis; RRMS = relapsing–remitting MS; SPMS = secondary progressive MS.

important factor. Specifically, we found that a 10-year increase in age was associated with a 9% increase in iron levels (95% CI = 1–17%, $p = 0.02$). This age effect was found to be essentially the same in both early active plaques and PPWM. Because our estimates depended on age, we chose 3 specific ages (20, 40, and 60 years) at which to report iron levels (see Table 3). Whereas the absolute concentrations of iron varied with age, the differences, CIs, and p values were not age dependent. The statistically significant difference between the iron content of IP II and IP III early active lesions was maintained even when the outlier (Case 4, IP II in Fig 3A) was omitted, in which case IP II early active lesions had 31% more iron than IP III early active lesions (95% CI = 6–64%, $p = 0.01$).

Among IP II patients, we found that the iron content of early active IP II lesions was 30% higher than that of the PPWM (95% CI = 3–64%, $p = 0.03$). In contrast, among IP III patients, iron levels of early active lesions were 28% lower than those of the PPWM (95% CI = −40 to −14%, $p < 0.001$). When normalizing the iron content of early active lesions to that of the surrounding PPWM, the ratio was significantly higher in IP II patients ($p < 0.001$; see Fig 3C).

Distribution of Iron

Microfocused XFI showed that iron in early active IP II lesions localized to macrophages when iron maps were compared to the adjacent immunohistochemically stained sections (see Fig 4). Macrophages in early active IP III

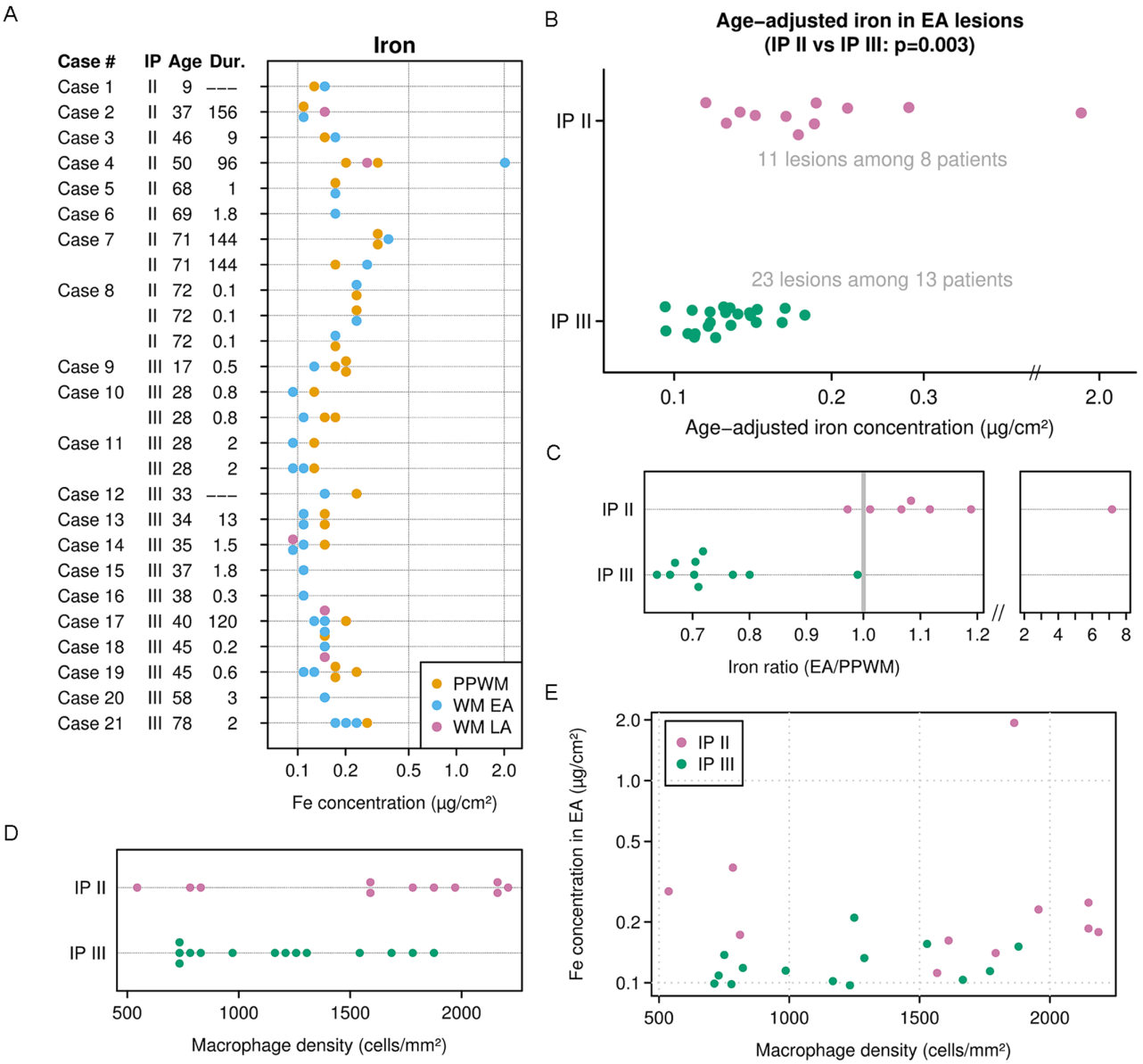

FIGURE 3: Early active (EA) immunopattern (IP) II lesions contain significantly more iron than EA IP III lesions. (A) Distribution of iron concentrations for each of the 26 blocks in the study. Each point represents one region of interest (ROI) on a particular block. The value displayed for each ROI is the median concentration over the entire ROI shown on a log-transformed scale. The subject age (years) and disease duration (Dur.; months) are provided on the y-axis, noting that 4 subjects have multiple blocks. (B) Age-adjusted iron concentration on the log scale by IP in EA lesions. The data are shown as the iron concentration found in the ROI minus the contribution attributed to age relative to the median age of 40 years. A broken x-axis is used to include the highest value of 1.9. In sensitivity analyses that omitted this individual age-adjusted iron remained higher in pattern II versus pattern III (p = 0.01). (C) Distribution of the EA/periplaque white matter (PPWM) iron ratio by IP classification ($p < 0.001$, Wilcoxon rank sum/Mann–Whitney U test). Each point in the figure represents the within-subject ratio of EA iron to PPWM iron. Note the break in the x-axis. (D) Distribution of macrophage densities in IP II versus IP III. We do not find a statistically significant difference in the distribution of macrophage densities between IP II and IP III (p = 0.11). (E) Relationship of iron concentration (y-axis) to macrophage density (x-axis). The colored dots represent IP II (purple) and IP III (green). We do not find a significant association between iron concentration and macrophage density overall (p = 0.74), within IP II (p = 0.88), nor within IP III (p = 0.30). LA = late active; WM = white matter.

lesions contained little iron. Overall, the macrophage density in IP II (1,573 cells/mm^2, 95% CI = 1,227–1,920) and IP III (1,233 cells/mm^2, 95% CI = 800–1,188) did not differ significantly (p = 0.4; see Fig 3D). Furthermore, we did not find a significant relationship between iron concentration and macrophage density overall (p = 0.20), within IP II (p = 0.88), or within IP III (p = 0.30) lesions (see Fig 3E). The PPWM of both patterns showed a patchy distribution of iron (see Fig 4E, G) consistent with the iron being localized to myelin and oligodendrocyes,[28] although a more punctuated appearance of iron in the IP II PPWM (see Fig 4E) suggested that microglia in IP II

TABLE 3. Comparing IP II and IP III on Iron by Early Active, Late Active, and PPWM

Tissue	IP II	IP III	Difference	*p*
Early active				0.004
Age 20 yr	0.17 (0.12–0.25)	0.11 (0.08–0.13)	64% (17 to 127%)	
Age 40 yr	0.21 (0.16–0.27)	0.13 (0.11–0.15)	64% (17 to 127%)	
Age 60 yr	0.25 (0.19–0.32)	0.15 (0.12–0.19)	64% (17 to 127%)	
Late active				0.40
Age 20 yr	0.14 (0.08–0.23)	0.11 (0.07–0.16)	29% (−29 to 130%)	
Age 40 yr	0.16 (0.10–0.26)	0.13 (0.09–0.18)	29% (−29 to 130%)	
Age 60 yr	0.19 (0.12–0.31)	0.15 (0.10–0.23)	29% (−29 to 130%)	
PPWM				0.54
Age 20 yr	0.13 (0.09–0.19)	0.15 (0.12–0.19)	−10% (−36 to 25%)	
Age 40 yr	0.16 (0.12–0.21)	0.18 (0.14–0.22)	−10% (−36 to 25%)	
Age 60 yr	0.19 (0.15–0.24)	0.21 (0.16–0.28)	−10% (−36 to 25%)	

Values shown are groupwise geometric means expressed in $\mu g/cm^2$ with 95% confidence intervals, differences for IP II compared to IP III on a percentage scale with 95% confidence intervals, and *p* value for the difference. Mean iron levels depend on age, but the difference does not.
IP = immunopattern; PPWM = periplaque white matter.

PPWM contained more iron than microglia in IP III PPWM.

Chemically specific imaging of iron showed that only ferric (Fe^{3+}) iron was present (see Fig 4A, C, E, G), whereas ferrous (Fe^{2+}) iron was unremarkable in lesions (see Fig 4B, D) and PPWM (see Fig 4F, H) of both IPs.

H-Ferritin was abundant in macrophages that infiltrated IP II early active lesions (see Fig 5A). In IP III lesions, areas of robust macrophage H-ferritin immunoreactivity alternated with areas where macrophages did not show immunoreactivity for H-ferritin or contained only few cytoplasmic H-ferritin immunopositive puncta (see Fig 5B). Myelin, oligodendrocytes (see lower left inset in Fig. 5C and lower insets in Fig. 5D), and microglia (see upper insets in Fig. 5C, D) in PPWM were immunoreactive for H-ferritin. In IP II PPWM, oligodendrocyte H-ferritin immunoreactivity appeared as a brown rim around the H-ferritin immunonegative nucleus, although not all oligodendrocytes were immunopositive for H-ferritin (see lower inset in Fig 5C). In IP III PPWM, H-ferritin immunohistochemistry stained the nuclei of most oligodendrocytes (see Fig 5D).

Discussion

Our study shows that distribution and content of iron are heterogeneous in early active MS lesions, and differ between IP II and IP III MS subtypes. Using cutting edge X-ray fluorescence synchrotron imaging that is sensitive and specific to iron,[24] we report that IP II early active lesions contain significantly more iron than IP III early active lesions, and that iron localizes in macrophages. These findings are also supported by our observations that H-ferritin protein expression is abundant only in macrophages in IP II lesions. We did not find a statistically significant difference between macrophage densities in IP II and IP III lesions, and the iron content did not correlate to the macrophage density, suggesting that there is a pronounced heterogeneity in iron loading of macrophages in early active MS lesions, which appears independent of the number of macrophages, demyelinating activity, myelin phagocytosis, and topographical region. This indicates there are factors contributing to the differential propensity for macrophages to accumulate and/or release iron and that iron dyshomeostasis may play an important role in the pathogenesis and evolution of MS lesions.

It has been suggested that macrophages and microglia in early MS accumulate iron that is released from destroyed oligodendrocytes.[18] Although macrophages are present and abundant in both IP II and IP III active MS lesions, only those present in IP II lesions accumulated large amounts of iron. This indicates that other factors, in addition to the previously suggested iron storage

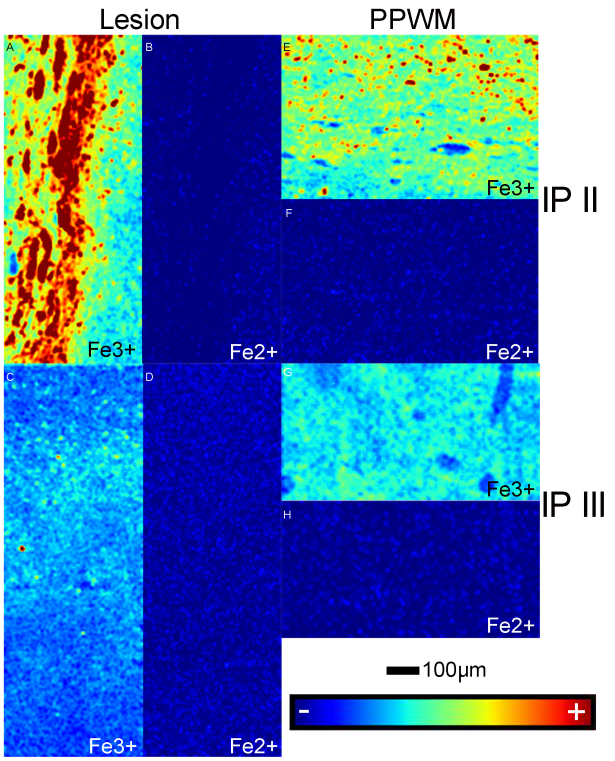

FIGURE 4: Microfocused X-ray fluorescence imaging of early active lesions. (A) Ferric iron (Fe^{3+}) in immunopattern (IP) II early active lesions is increased and localized within macrophages. (B) Ferrous iron (Fe^{2+}) in IP II early active lesions is unremarkable. (C) Ferric iron in IP III early active lesions is decreased. (D) Ferrous iron in IP III early active lesions is unremarkable. (E) There is less ferric iron in the periplaque white matter (PPWM) than in lesions of IP II patients. (F) Ferrous iron in IP II PPWM is unremarkable. (G) There is more ferric iron in the PPWM than in lesions of IP III patients. (H) Ferrous iron in IP III PPWM is unremarkable. Color scales (A–H) represent the normalized total Kα fluorescence counts, proportional to total metal present, from blue (lowest) to red (highest). Scale bar = 100µm.

shift from destroyed oligodendrocytes to macrophages and microglia, affect how macrophages accumulate or release iron.

One explanation is that the heterogeneous iron loading of macrophages reflects their different polarization states.[19,29] Polarization is a spectrum of functional profiles macrophages adopt depending on signals received from the inflammatory environment. At one end of the spectrum, classically activated (M1-polarized) macrophages accumulate and sequester iron safely in ferritin, similarly to the macrophages we describe in IP II lesions and that are associated with production of reactive oxygen species (ROS) and proinflammatory cytokines.[30,31] At the opposing end of the spectrum, alternatively activated (M2-polarized) macrophages have low intracellular iron and decreased ferritin levels,[31] similarly to the IP III macrophages. Reduced intracellular iron availability blocks the formation of iron-dependent enzymes involved in the inflammatory response, dampens inflammation, and promotes tissue repair.[30] Because iron is a required cofactor for enzymes that degrade HIF-1α,[32] macrophage iron deficiency could mimic the effects of hypoxia, a feature characteristic of IP III MS lesions.[33,34] Such an iron-related macrophage polarization dichotomy has been described, but attributed to the macrophage's ability to phagocytose either iron or myelin; iron phagocytosis induces a proinflammatory M1-polarization state, whereas myelin phagocytosis prevents iron uptake, converting macrophages to an anti-inflammatory M2-polarization state.[19] A previous observation,[18] supported by our findings, is that phagocytosis of iron and of myelin by macrophages is not mutually exclusive. Recent studies have suggested that although the difference in macrophage and microglia polarization may not be pronounced between IP II and IP III lesions, it is the origin of macrophages that differs; IP II lesions contain a larger proportion of recruited myeloid cells.[35] These findings coupled with possibly more severe blood–brain barrier dysfunction and leakage of transferrin-bound and non–transferrin-bound iron in IP II lesions,[36] and with the monocyte-derived macrophages' superior ability to remove damaged and senescent erythrocytes,[37] may also explain why phagocytic cells in IP II lesions contain more iron than those in IP III lesions.

Another explanation is that iron heterogeneity is an expression of the different demyelination mechanisms postulated to occur in different IPs. Demyelination in IP II MS is likely caused by complement activating antibodies targeting yet unknown antigens on oligodendrocytes and/or myelin. Accordingly, there is a striking colocalization of antibody deposition and complement activation on myelin and within myelin-laden macrophages in IP II MS.[2,38,39] The complement component C1q increases its binding to immunoglobulins in the presence of iron.[40] C5 also binds iron, which is required for converting C5 to activated C5b by hydroxyl radicals,[41] an essential step in the formation of the membrane attack complex. Thus, iron is essential for complement function and terminal lytic complex assembly, explaining perhaps why IP II MS macrophages that phagocytose complement-opsonized myelin debris contain increased iron.

In contrast, IP III MS lesions may result from disturbances in oligodendrocytes, initiating an "inside-out" failure to maintain myelin and/or heighten the vulnerability of oligodendrocytes to the toxicity of inflammatory mediators.[2] Oxidative stress and mitochondrial injury play an important role in the pathogenesis of IP III MS,[5,6,42] and it has been assumed that excess iron partially drives tissue injury in IP III MS. Our results, however, suggest that iron deficiency, rather than the excess of iron, may drive the pathology of IP III lesions. Iron is essential for

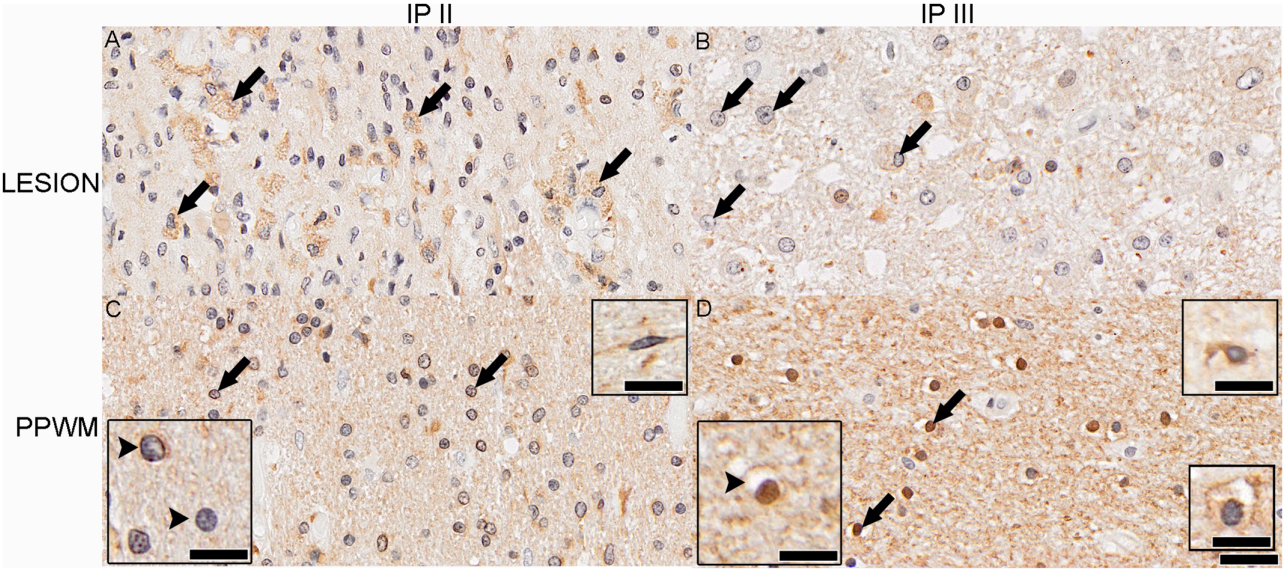

FIGURE 5: H-Ferritin protein expression in lesions and periplaque white matter (PPWM). (A) H-Ferritin is abundant in macrophages present in immunopattern (IP) II early active lesions. Arrows indicate representative macrophages with high H-ferritin immunoreactivity. (B) H-Ferritin immunoreactivity is weak in macrophages (some exemplified by *arrows*) that infiltrate IP III early active lesions. (C) Myelin, oligodendrocytes (*arrows*), and microglia (*upper inset*) are immunoreactive for H-ferritin in IP II PPWM. However, not all oligodendrocytes express H-ferritin; the upper arrowhead in the lower inset shows an oligodendrocyte immunoreactive for H-ferritin, whereas the lower arrowhead indicates an H-ferritin–negative oligodendrocyte. (D) Myelin, most oligodendrocyte nuclei (*arrows, lower left inset*), and microglia (*upper inset*) are immunoreactive for H-ferritin in IP III PPWM. Few oligodendrocytes (*lower right inset*) have H-ferritin–immunonegative nuclei. Scale bar = 50μm. Inset scale bars = 25μm.

energy production, because it functions as a cofactor for cytochromes and iron–sulfur clusters of the mitochondrial respiratory chain.[28] Iron depletion, as observed in IP III lesions, can disrupt the iron–sulfur cluster biogenesis and oxidative phosphorylation with increased electron escape from the mitochondrial respiratory chain, and subsequent increased mitochondrial oxidative damage, decreased energy production, and a state of virtual hypoxia.[6,33,43] We have also found that H-ferritin in IP III, but not IP II, lesions localizes to nuclei of oligodendrocytes consistent with the translocation of H-ferritin from the cytoplasm to the nucleus, where it binds to the DNA to protect it from ROS-induced damage.[44–46] This suggests that oxidative damage is already present and more extensive in the IP III than IP II PPWM.

MS is clinically, genetically, radiographically, and pathologically heterogeneous. The challenge now is identifying surrogate magnetic resonance imaging (MRI), clinical, genetic, serological, and/or cerebrospinal fluid markers that correlate with IPs in the nonbiopsied MS patient population. We show here that IP II MS lesions contain significantly more iron than IP III lesions, and this novel observation paves the way for developing new or using existing iron-sensitive MRI techniques[17,19,47–53] to stratify patients with early MS. In a clinical MRI setting, it is challenging to define what is "more" or "less" iron, because the normal brain iron content varies with age[54] and perhaps with other factors such as genetic background and diet.[55,56] However, as shown here, the PPWM, the white matter immediately adjacent to the lesion, is an appropriate internal control, and we suggest that the ratio of lesional iron to the PPWM iron (which can only be <1 or >1; see Fig 3C) represents a better stratification marker than the absolute amount of iron found in lesions.

The relatively small number of cases used is the main limitation of our study, and further studies need to establish whether our findings are broadly applicable in a larger cohort of immunophenotyped MS patients. The number of cases analyzed in our study was restricted mainly by the availability of synchrotron beamtime, but also by the tissue availability (ie, for each imaged slide, enough additional slides to support both the general pathological evaluation and the immunophenotyping had to be available).

An obvious practical application of the heterogeneity concept is the design of novel therapeutic strategies specifically tailored to each IP. In support of this hypothesis, IP II MS is uniquely responsive to plasma exchange for treatment of steroid-unresponsive fulminant MS relapses, whereas this treatment does not benefit IP III MS patients.[8] Iron chelation therapy in MS stems from the premise that iron accumulates in MS lesions. Our results, however, argue against indiscriminate iron chelation in patients with acute MS. Chelation therapy may be beneficial in IP II MS, where it may impair the formation of the terminal lytic complex protecting oligodendrocytes and

myelin. However, the chelation of the minimal amounts of iron present in IP III MS may suppress the already challenged metabolic activity of oligodendrocytes, thereby accelerating their death.[57]

Acknowledgments

This study was funded by the Canada Research Chairs Program (to B.F.P.), the Saskatchewan Health Research Foundation (to B.F.P.), Biogen Idec (to B.F.P. and C.F.L.), and the National Institute of Neurological Disorders and Stroke (NINDS), NIH (to C.F.L.). M.T. and R.C.A. were Fellows of the Canadian Institutes of Health Research Training grant in Health Research Using Synchrotron Techniques (CIHR-THRUST). M.T. was supported by a College of Medicine Graduate Scholarship, University of Saskatchewan and a Saskatchewan Innovation and Opportunity Scholarship, Government of Saskatchewan. J.M.F. was supported by the Austrian Science Fund (FWF Project J3508-B24) while conducting parts of this work. Use of the Stanford Synchrotron Radiation Lightsource, SLAC National Accelerator Laboratory, is supported by the US Department of Energy, Office of Science, Office of Basic Energy Sciences under Contract No. DE-AC02-76SF00515. The SSRL Structural Molecular Biology Program is supported by the DOE Office of Biological and Environmental Research, and by the NIH National Institute of General Medical Sciences (NIGMS; including P41GM103393). The contents of this publication are solely the responsibility of the authors and do not necessarily represent the official views of the NIGMS or NIH.

We thank A. Givens and P. Ziemer for their expert technical assistance, and the Department of Pathology and Laboratory Medicine, Saskatoon Health Region, Saskatoon, Canada for retrieval of some of the tissue blocks used in this study.

Author Contributions

B.F.P. and C.F.L. contributed to the conception and design of the study. M.T., J.M.F., S.D.W., P.D.F.-G., S.M.W., Y.G., R.C.A., C.A.R., W.B., H.L., K.L.F., M.J.P., J.E.P., C.F.L., and B.F.P. contributed to the acquisition and analysis of data. B.F.P., M.T., and C.F.L. contributed to drafting the text and preparing the figures.

Potential Conflicts of Interest

Nothing to report.

References

1. Poser S, Raun NE, Poser W. Age at onset, initial symptomatology and the course of multiple sclerosis. Acta Neurol Scand 1982;66: 355–362.
2. Lucchinetti C, Bruck W, Parisi J, et al. Heterogeneity of multiple sclerosis lesions: implications for the pathogenesis of demyelination. Ann Neurol 2000;47:707–717.
3. Metz I, Weigand SD, Popescu BF, et al. Pathologic heterogeneity persists in early active multiple sclerosis lesions. Ann Neurol 2014; 75:728–738.
4. Mahad DJ, Trebst C, Kivisakk P, et al. Expression of chemokine receptors CCR1 and CCR5 reflects differential activation of mononuclear phagocytes in pattern II and pattern III multiple sclerosis lesions. J Neuropathol Exp Neurol 2004;63:262–273.
5. Mahad D, Ziabreva I, Lassmann H, Turnbull D. Mitochondrial defects in acute multiple sclerosis lesions. Brain 2008;131:1722–1735.
6. Haider L, Fischer MT, Frischer JM, et al. Oxidative damage in multiple sclerosis lesions. Brain 2011;134:1914–1924.
7. Marik C, Felts PA, Bauer J, et al. Lesion genesis in a subset of patients with multiple sclerosis: a role for innate immunity? Brain 2007;130:2800–2815.
8. Keegan M, Konig F, McClelland R, et al. Relation between humoral pathological changes in multiple sclerosis and response to therapeutic plasma exchange. Lancet 2005;366:579–582.
9. Stork L, Ellenberger D, Beissbarth T, et al. Differences in the reponses to apheresis therapy of patients with 3 histopathologically classified immunopathological patterns of multiple sclerosis. JAMA Neurol 2018;75:428–435.
10. Arrambide G, Iacobaeus E, Amato MP, et al. Aggressive multiple sclerosis (2): treatment. Mult Scler 2020;26:1352458520924595.
11. Greenfield AL, Hauser SL. B-cell therapy for multiple sclerosis: entering an era. Ann Neurol 2018;83:13–26.
12. Barnett MH, Prineas JW. Relapsing and remitting multiple sclerosis: pathology of the newly forming lesion. Ann Neurol 2004;55: 458–468.
13. Breij EC, Brink BP, Veerhuis R, et al. Homogeneity of active demyelinating lesions in established multiple sclerosis. Ann Neurol 2008; 63:16–25.
14. Ingram G, Loveless S, Howell OW, et al. Complement activation in multiple sclerosis plaques: an immunohistochemical analysis. Acta Neuropathol Commun 2014;2:53.
15. Bruck W, Popescu B, Lucchinetti CF, et al. Neuromyelitis optica lesions may inform multiple sclerosis heterogeneity debate. Ann Neurol 2012;72:385–394.
16. Frischer JM, Weigand SD, Guo Y, et al. Clinical and pathological insights into the dynamic nature of the white matter multiple sclerosis plaque. Ann Neurol 2015;78:710–721.
17. Bagnato F, Hametner S, Boyd E, et al. Untangling the R2* contrast in multiple sclerosis: a combined MRI-histology study at 7.0 tesla. PLoS One 2018;13:e0193839.
18. Hametner S, Wimmer I, Haider L, et al. Iron and neurodegeneration in the multiple sclerosis brain. Ann Neurol 2013;74:848–861.
19. Mehta V, Pei W, Yang G, et al. Iron is a sensitive biomarker for inflammation in multiple sclerosis lesions. PLoS One 2013;8:e57573.
20. Popescu BF, Frischer JM, Webb SM, et al. Pathogenic implications of distinct patterns of iron and zinc in chronic MS lesions. Acta Neuropathol 2017;134:45–64.
21. McDonald WI, Compston A, Edan G, et al. Recommended diagnostic criteria for multiple sclerosis: guidelines from the International Panel on the Diagnosis of Multiple Sclerosis. Ann Neurol 2001;50: 121–127.

22. Poser CM, Paty DW, Scheinberg L, et al. New diagnostic criteria for multiple sclerosis: guidelines for research protocols. Ann Neurol 1983;13:227–231.
23. Bruck W, Porada P, Poser S, et al. Monocyte/macrophage differentiation in early multiple sclerosis lesions. Ann Neurol 1995;38:788–796.
24. Pushie MJ, Pickering IJ, Korbas M, et al. Elemental and chemically specific X-ray fluorescence imaging of biological systems. Chem Rev 2014;114:8499–8541.
25. Webb SM. The MicroAnalysis toolkit: X-ray fluorescence image processing software. Am Inst Phys Conf Proc 2011;1365:196–199.
26. Pushie MJ, Crawford AM, Sylvain NJ, et al. Revealing the penumbra through imaging elemental markers of cellular metabolism in an ischemic stroke model. ACS Chem Neurosci 2018;9:886–893.
27. Gelman A, Hill J. *Data analysis using regression and multilevel/hierarchical models*. 1st ed, Cambridge, UK: Cambridge University Press, 2006.
28. Todorich B, Pasquini JM, Garcia CI, et al. Oligodendrocytes and myelination: the role of iron. Glia 2009;57:467–478.
29. Corna G, Campana L, Pignatti E, et al. Polarization dictates iron handling by inflammatory and alternatively activated macrophages. Haematologica 2010;95:1814–1822.
30. Cairo G, Recalcati S, Mantovani A, Locati M. Iron trafficking and metabolism in macrophages: contribution to the polarized phenotype. Trends Immunol 2011;32:241–247.
31. Gammella E, Buratti P, Cairo G, Recalcati S. Macrophages: central regulators of iron balance. Metallomics 2014;6:1336–1345.
32. Peyssonnaux C, Nizet V, Johnson RS. Role of the hypoxia inducible factors HIF in iron metabolism. Cell Cycle 2008;7:28–32.
33. Aboul-Enein F, Bauer J, Klein M, et al. Selective and antigen-dependent effects of myelin degeneration on central nervous system inflammation. J Neuropathol Exp Neurol 2004;63:1284–1296.
34. Stadelmann C, Ludwin S, Tabira T, et al. Tissue preconditioning may explain concentric lesions in Balo's type of multiple sclerosis. Brain 2005;128:979–987.
35. Zrzavy T, Hametner S, Wimmer I, et al. Loss of 'homeostatic' microglia and patterns of their activation in active multiple sclerosis. Brain 2017;140:1900–1913.
36. Hochmeister S, Grundtner R, Bauer J, et al. Dysferlin is a new marker for leaky brain blood vessels in multiple sclerosis. J Neuropathol Exp Neurol 2006;65:855–865.
37. Chang CF, Goods BA, Askenase MH, et al. Erythrocyte efferocytosis modulates macrophages towards recovery after intracerebral hemorrhage. J Clin Invest 2018;128:607–624.
38. Barnett MH, Parratt JD, Cho ES, Prineas JW. Immunoglobulins and complement in postmortem multiple sclerosis tissue. Ann Neurol 2009;65:32–46.
39. Storch MK, Piddlesden S, Haltia M, et al. Multiple sclerosis: in situ evidence for antibody- and complement-mediated demyelination. Ann Neurol 1998;43:465–471.
40. Dimitrov JD, Roumenina LT, Doltchinkova VR, Vassilev TL. Iron ions and haeme modulate the binding properties of complement subcomponent C1q and of immunoglobulins. Scand J Immunol 2007;65:230–239.
41. Vogi W, Nolte R, Brunahl D. Binding of iron to the 5th component of human complement directs oxygen radical-mediated conversion to specific sites and causes nonenzymic activation. Complement Inflamm 1991;8:313–319.
42. van Horssen J, Schreibelt G, Drexhage J, et al. Severe oxidative damage in multiple sclerosis lesions coincides with enhanced antioxidant enzyme expression. Free Radic Biol Med 2008;45:1729–1737.
43. Higgins GC, Beart PM, Shin YS, et al. Oxidative stress: emerging mitochondrial and cellular themes and variations in neuronal injury. J Alzheimers Dis 2010;20:S453–S473.
44. Alkhateeb AA, Connor JR. Nuclear ferritin: a new role for ferritin in cell biology. Biochim Biophys Acta 2010;1800:793–797.
45. Cai C, Ching A, Lagace C, Linsenmayer T. Nuclear ferritin-mediated protection of corneal epithelial cells from oxidative damage to DNA. Dev Dyn 2008;237:2676–2683.
46. Cai CX, Birk DE, Linsenmayer TF. Nuclear ferritin protects DNA from UV damage in corneal epithelial cells. Mol Biol Cell 1998;9:1037–1051.
47. Absinta M, Sati P, Reich DS. Advanced MRI and staging of multiple sclerosis lesions. Nat Rev Neurol 2016;12:358–368.
48. Absinta M, Sati P, Schindler M, et al. Persistent 7-tesla phase rim predicts poor outcome in new multiple sclerosis patient lesions. J Clin Invest 2016;126:2597–2609.
49. Bagnato F, Hametner S, Welch EB. Visualizing iron in multiple sclerosis. Magn Reson Imaging 2013;31:376–384.
50. Stüber C, Pitt D, Wang Y. Iron in multiple sclerosis and its noninvasive imaging with quantitative susceptibility mapping. Int J Mol Sci 2016;17:100.
51. Zhang Y, Gauthier SA, Gupta A, et al. Quantitative susceptibility mapping and R2* measured changes during white matter lesion development in multiple sclerosis: myelin breakdown, myelin debris degradation and removal, and iron accumulation. AJNR Am J Neuroradiol 2016;37:1629–1635.
52. Zheng W, Haacke EM, Webb SM, Nichol H. Imaging of stroke: a comparison between X-ray fluorescence and magnetic resonance imaging methods. Magn Reson Imaging 2012;30:1416–1423.
53. Zheng W, Nichol H, Liu S, et al. Measuring iron in the brain using quantitative susceptibility mapping and X-ray fluorescence imaging. Neuroimage 2013;78:68–74.
54. Zecca L, Youdim MB, Riederer P, et al. Iron, brain ageing and neurodegenerative disorders. Nat Rev Neurosci 2004;5:863–873.
55. Bartzokis G, Lu PH, Tishler TA, et al. Prevalent iron metabolism gene variants associated with increased brain ferritin iron in healthy older men. J Alzheimers Dis 2010;20:333–341.
56. Hagemeier J, Tong O, Dwyer MG, et al. Effects of diet on brain iron levels among healthy individuals: an MRI pilot study. Neurobiol Aging 2015;36:1678–1685.
57. Zhang X, Haaf M, Todorich B, et al. Cytokine toxicity to oligodendrocyte precursors is mediated by iron. Glia 2005;52:199–208.